

*Electronic Supplementary Information for*

## **Surface and grain boundary energy as the key enabler to ferroelectricity in nanoscale hafnia-zirconia: comparison of model and experiment**

Min Hyuk Park,<sup>a,b</sup> Young Hwan Lee,<sup>a</sup> Han Joon Kim,<sup>a</sup> Tony Schenk,<sup>b</sup> Woongkyu Lee,<sup>a</sup> Keum Do Kim,<sup>a</sup> Franz P. G. Fengler,<sup>b</sup> Thomas Mikolajick,<sup>b,c</sup> Uwe Schroeder,<sup>b,\*</sup> and Cheol Seong Hwang<sup>a,#</sup>

<sup>1</sup>Department of Material Science & Engineering and Inter-university Semiconductor Research Center, Seoul National University, Seoul 151-744, Korea.

<sup>2</sup>NaMLab gGmbH, Noethnitzer Strasse 64, 01187 Dresden, Germany.

<sup>3</sup>Chair of Nanoelectronic Materials, TU Dresden, 01062 Dresden, Germany.

(e-mails: \*[Uwe.Schroeder@namlab.com](mailto:Uwe.Schroeder@namlab.com), #[cheolsh@snu.ac.kr](mailto:cheolsh@snu.ac.kr) )

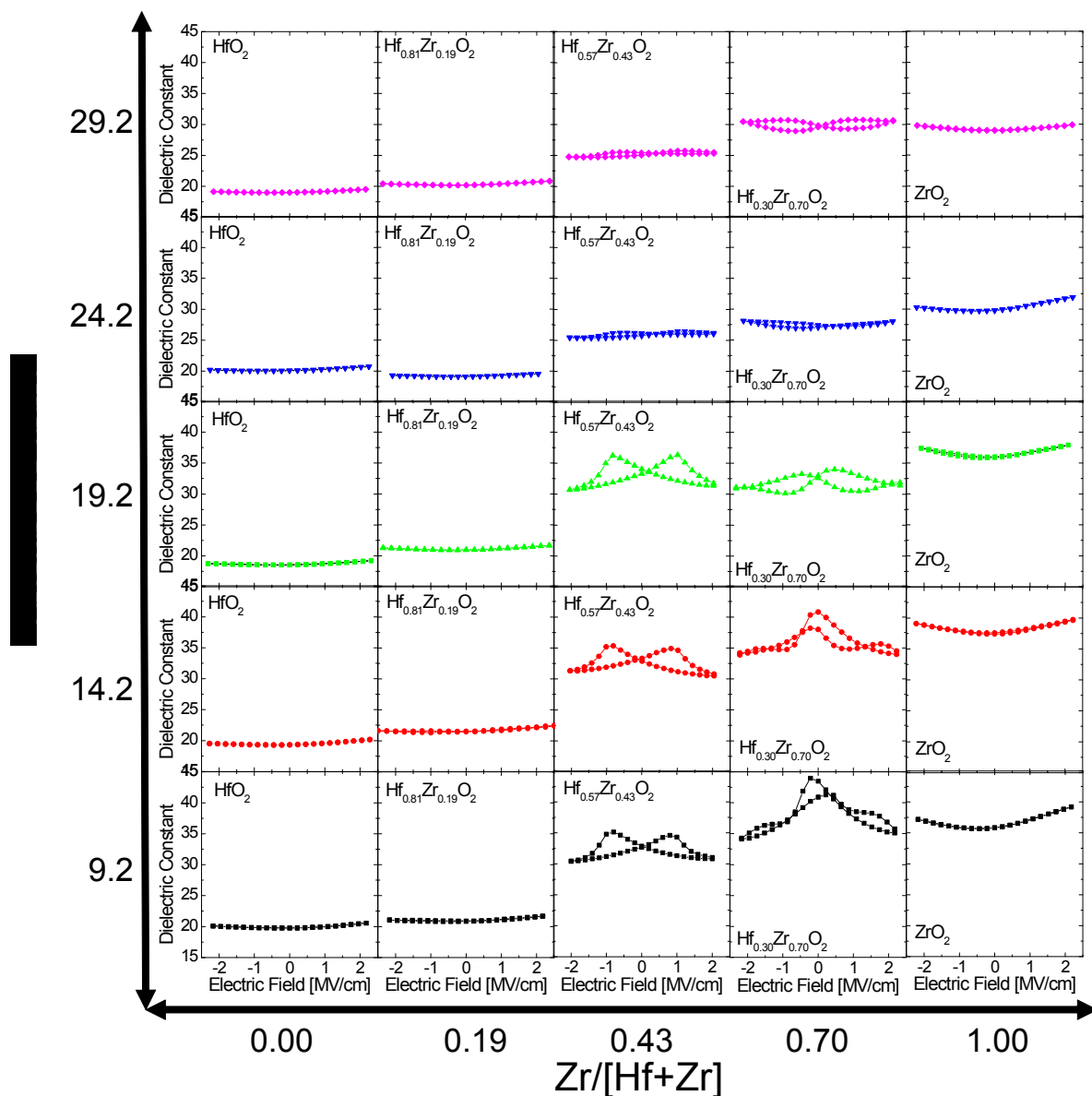


**Figure S1.** The dielectric constant – electric field curves of HZO films with various composition ( $\text{Zr}/[\text{Zr}+\text{Hf}] = 0.00, 0.19, 0.43, 0.70, 1.00$ ) and thickness ( $\sim 9.2, 14.2, 19.2, 24.2$ , and  $29.2$  nm).

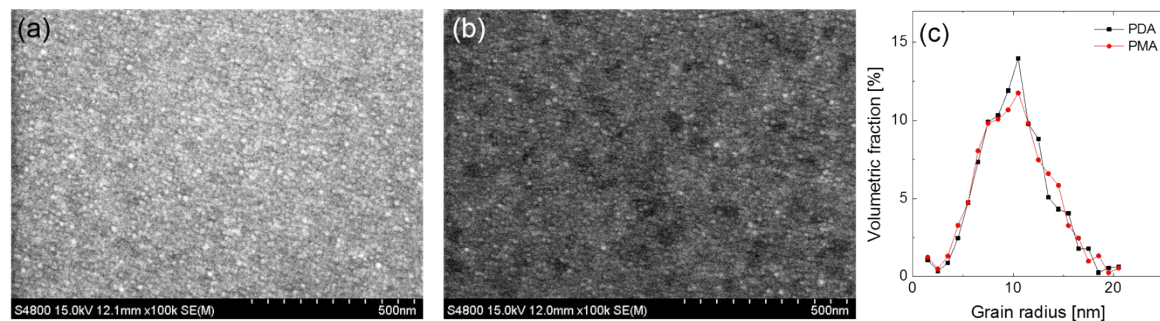


**Figure S2.** Plan-view scanning electron microscopy images of 9.1 nm-thick  $\text{Hf}_{0.48}\text{Zr}_{0.52}\text{O}_2$  film annealed using (a) post-deposition-annealing (PDA) and (b) post-metallization-annealing (PMA). TiN top electrode was removed by wet etching. (c) Grain size distribution of the 9.1 nm-thick PDA and PMA  $\text{Hf}_{0.48}\text{Zr}_{0.52}\text{O}_2$  films (extracted from figures S2a and b).

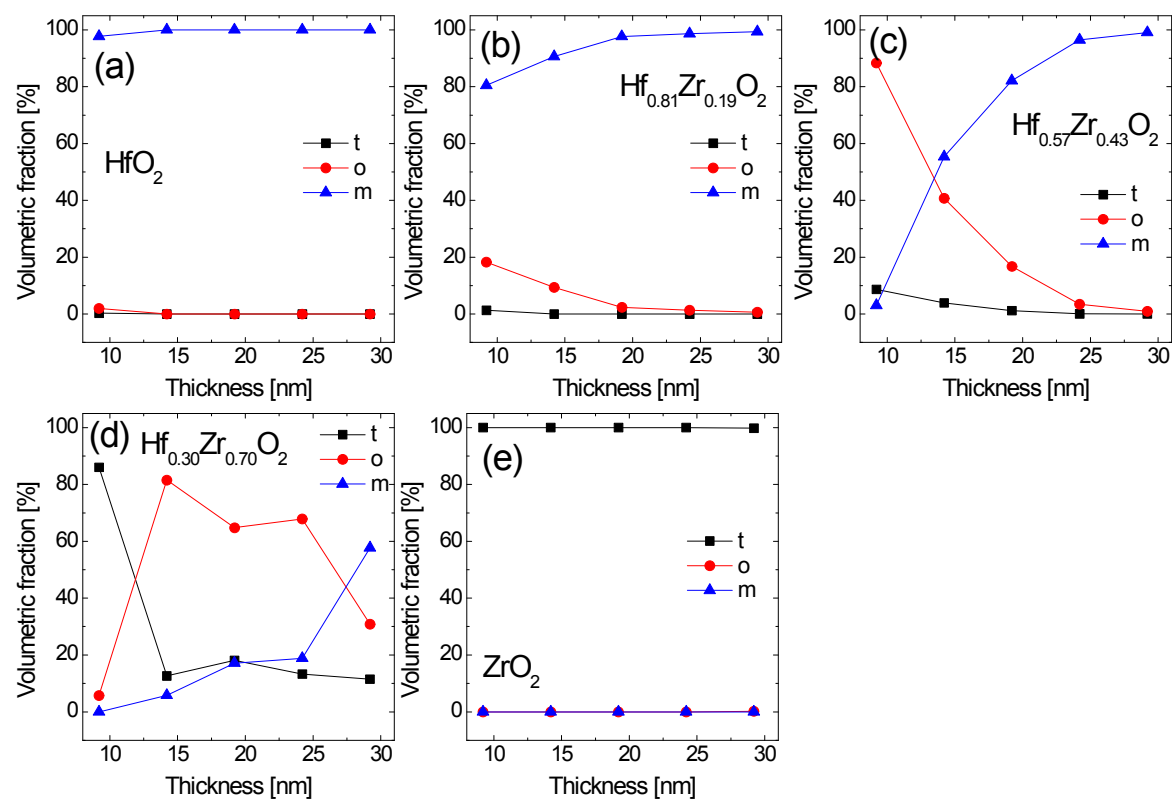


**Figure S3.** Changes in relative phase fractions estimated based on surface energy model in (a)  $\text{HfO}_2$ , (b)  $\text{Hf}_{0.81}\text{Zr}_{0.19}\text{O}_2$ , (c)  $\text{Hf}_{0.57}\text{Zr}_{0.43}\text{O}_2$ ,  $\text{Hf}_{0.30}\text{Zr}_{0.70}\text{O}_2$ , and (e)  $\text{ZrO}_2$  thin films with varying film thickness. (t: tetragonal; o: orthorhombic; m: monoclinic)

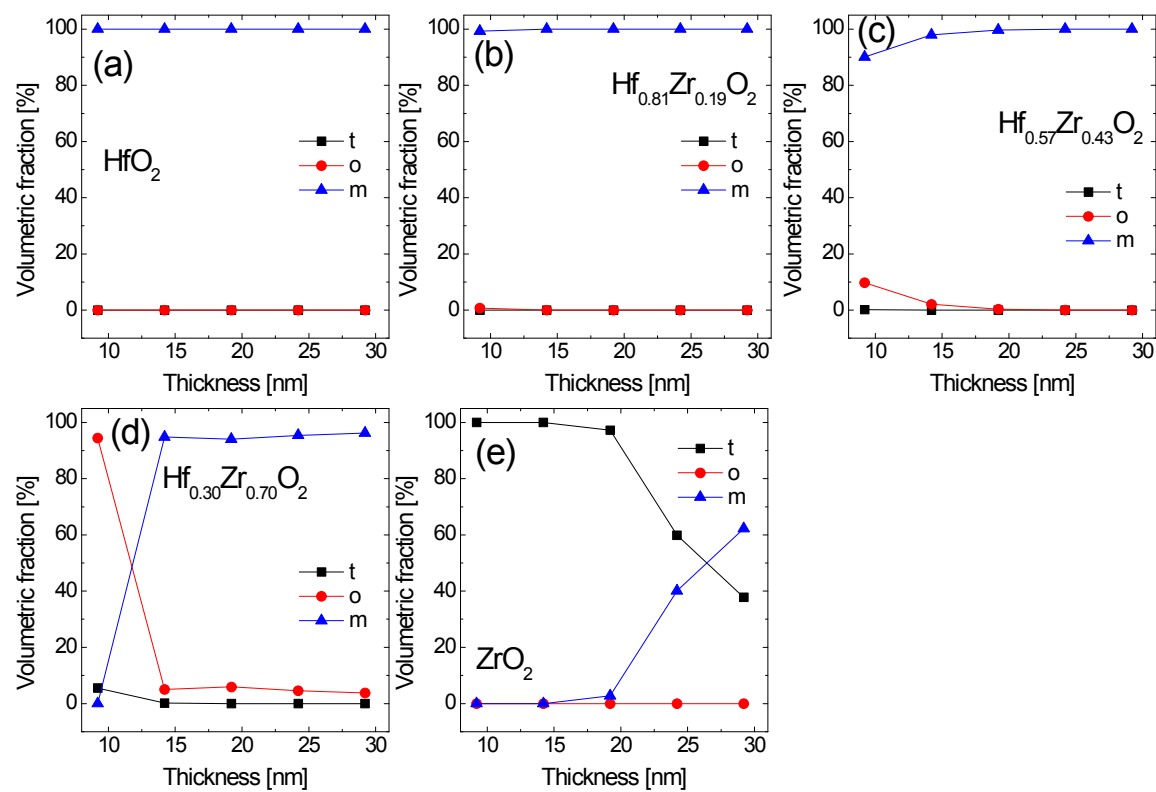


**Figure S4.** Changes in relative phase fractions estimated based on surface energy model with an assumption of interfacial energy = 0.33 surface energy in (a)  $\text{HfO}_2$ , (b)  $\text{Hf}_{0.81}\text{Zr}_{0.19}\text{O}_2$ , (c)  $\text{Hf}_{0.57}\text{Zr}_{0.43}\text{O}_2$ , (d)  $\text{Hf}_{0.30}\text{Zr}_{0.70}\text{O}_2$ , and (e)  $\text{ZrO}_2$  thin films with varying film thickness. (t: tetragonal; o: orthorhombic; m: monoclinic)

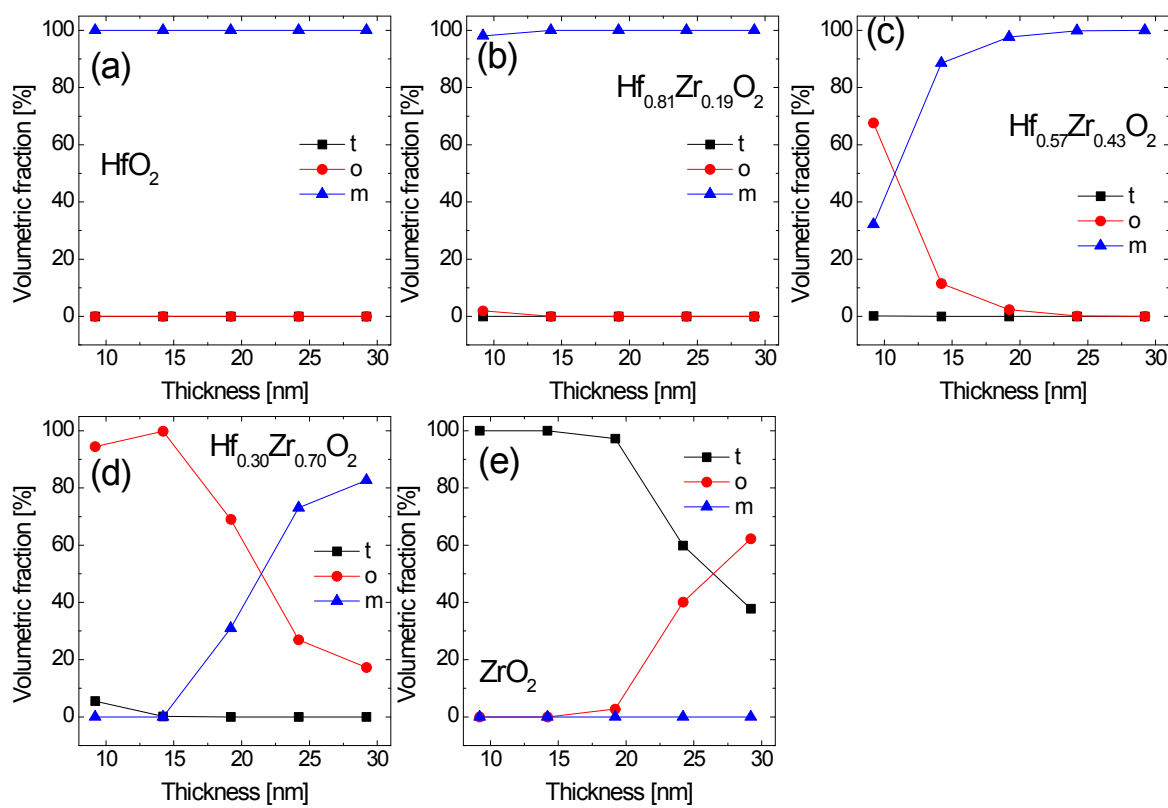


**Figure S5.** Changes in relative phase fractions estimated based on surface energy model with assumptions of interfacial energy = 0.33 surface energy and TiN capping effect for suppression of phase transition from tetragonal to monoclinic phase in (a)  $\text{HfO}_2$ , (b)  $\text{Hf}_{0.81}\text{Zr}_{0.19}\text{O}_2$ , (c)  $\text{Hf}_{0.57}\text{Zr}_{0.43}\text{O}_2$ ,  $\text{Hf}_{0.30}\text{Zr}_{0.70}\text{O}_2$ , and (e)  $\text{ZrO}_2$  thin films with varying film thickness. (t: tetragonal; o: orthorhombic; m: monoclinic)

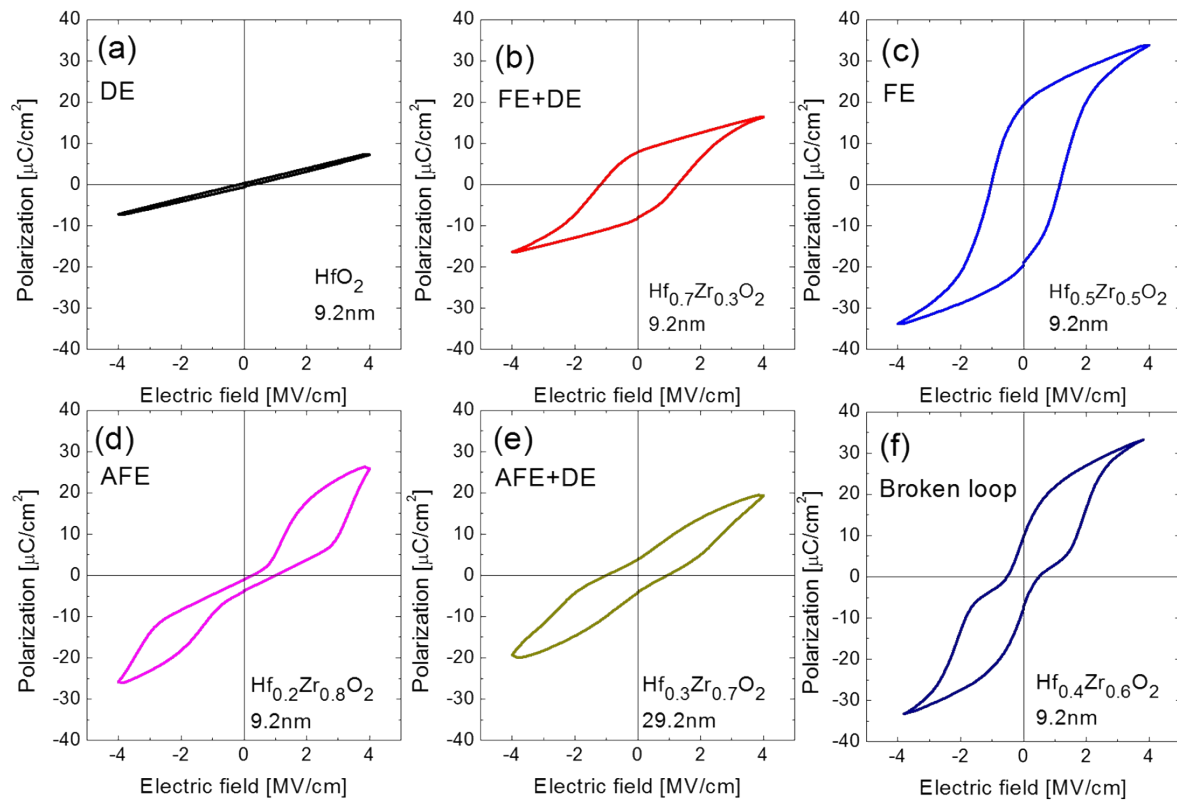


**Figure S6.** Exemplary polarization-electric field (P-E) curves for electrical performance diagram in figure 7 of the main text. Experimentally measured P-E curves of (a) 9.2 nm-thick HfO<sub>2</sub>, (b) 9.2 nm-thick Hf<sub>0.70</sub>Zr<sub>0.30</sub>O<sub>2</sub>, (c) 9.2 nm-thick Hf<sub>0.50</sub>Zr<sub>0.50</sub>O<sub>2</sub>, (d) 9.2 nm-thick Hf<sub>0.20</sub>Zr<sub>0.80</sub>O<sub>2</sub>, (e) 29.2 nm-thick Hf<sub>0.30</sub>Zr<sub>0.70</sub>O<sub>2</sub>, and (f) 9.2 nm-thick Hf<sub>0.40</sub>Zr<sub>0.60</sub>O<sub>2</sub> films. (DE: dielectric, FE: ferroelectric, AFE: antiferroelectric-like)